Check for updates

pH-Mediated nanoparticle dynamics in hydrogel nanocomposites†

Katie A. Rose, [a] Daeyeon Lee *[a] and Russell J. Composto *[abc]

The effect of static silica particles on the dynamics of quantum dot (QD) nanoparticles grafted with a poly(ethylene glycol) (PEG) brush in hydrogel nanocomposites is investigated using single particle tracking (SPT). At a low volume fraction of homogeneously dispersed silica ($\Phi = 0.005$), two distinct populations of PEG-QDs are observed, localized and mobile, whereas almost all PEG-QDs are mobile in neat hydrogel ($\Phi = 0.0$). Increasing the silica particle concentration ($\Phi = 0.01, 0.1$) results in an apparent change in the network structure, confounding the impact of silica on PEG-QD dynamics. The localized behavior of PEG-QDs is attributed to pH-mediated attraction between the PEG brush on the probe and surface silanol groups of silica. Using quartz crystal microbalance with dissipation (QCM-D), the extent of this interaction is investigated as a function of pH. At pH 5.8, the PEG brush on the probe can hydrogen bond with the silanol groups on silica, leading to adsorption of PEG-QDs. In contrast, at pH 9.2, silanol groups are deprotonated and PEG-QD is unable to hydrogen bond with silica leading to negligible adsorption. To test the effect of pH, PEG-QD dynamics are further investigated in hydrogel nanocomposites at $\Phi = 0.005$. SPT agrees with the QCM-D results; at pH 5.8, PEG-QDs are localized whereas at pH 9.2 the PEG-QDs are mobile. This study provides insight into controlling probe transport through hydrogel nanocomposites using pH-mediated interactions, with implications for tuning transport of nanoparticles underlying drug delivery and nanofiltration.

1 Introduction

Composed of both synthetic and natural polymers, hydrogels are 3D polymeric networks formed by physical or chemical crosslinks and swollen in water. They offer unique versatility in tuning their mechanical properties, swelling behavior and biocompatibility.[1–6] These properties have led to their usage in a broad range of applications, including in tissue engineering as hydrogel mechanical properties can be varied to match a large number of tissues,[7–9] as well as drug delivery[8,10] and filtration,[9,11–14] which utilize the physical and chemical constraints of the mesh on a drug, nanoparticle or other molecule to encapsulate and control their release. One of the most promising uses of hydrogels involve the synthesis of stimuli-responsive hydrogels that change their swelling and mechanical properties based on external stimuli such as temperature,[9,15–18]

pH[16,19,20] or light.[21,22] Using various polymer backbones or crosslinkers can achieve this stimuli-responsive behavior, such as using temperature responsive poly(N-isopropylacrylamide) or pH and salt responsive poly(acrylic acid) as the network, but this approach presents a challenge for applications in which a specific polymer network is desired. An alternative method to impart functionality while retaining the same polymer network is through the incorporation of nanoparticles, such as embedding magnetic nanoparticles into a hydrogel matrix for triggered drug release.[23–25] For numerous applications such as filtration and drug delivery, transport properties within hydrogel nanocomposites are critical. For example, nanoparticle-embedded silicone hydrogels have been explored in glaucoma therapy, where the incorporation of nanoparticles resulted in extended release time of a drug, timolol.[26] While these studies demonstrate the potential for the incorporation of nanoparticles we lack the fundamental understanding on how the transport of diffusing species is affected by their interactions with the components of nanocomposite hydrogel. Developing a deeper understanding of how the incorporation of nanoparticles into hydrogel composites changes dynamics of diffusing species will allow for targeted device design for therapeutics and other applications using hydrogel-nanocomposite materials.

The nanoscale structure and transport properties of hydrogels have been investigated by tracking the dynamics of nanoparticle

[a] *Department of Chemical and Biomolecular Engineering, University of Pennsylvania, Philadelphia, PA, 19104, USA. E-mail: daeyeon@seas.upenn.edu, composto@seas.upenn.edu*

[b] *Department of Materials Science and Engineering, University of Pennsylvania, Philadelphia, PA, 19104, USA*

[c] *Department of Bioengineering, University of Pennsylvania, Philadelphia, PA, 19104, USA*

† Electronic supplementary information (ESI) available. See DOI: 10.1039/d0sm02213f

probes. Broadly, nanoparticle dynamics in hydrogels are dependent on both the physical constraints of the polymeric network and chemical interactions between the probe and the network components. A previous report on nanoparticle dynamics in polyacrylamide highlights the importance of local polymer density on nanoprobe mobility; as the crosslinker concentration was increased, decreasing the mesh size, probe displacements decreased.[27] Our previous work which investigated the effect of heterogeneity of polyacrylamide gel on probe dynamics showed that the diffusion coefficient of nanoparticle probes in partially collapsed gels is greatly reduced due to the tortuous and heterogeneous pathway the probes experience.[28] The importance of attraction and binding interactions of a probe to biological networks such as biofilms[29–33] and cell membranes,[34–37] as well as synthetic hydrogel networks[15,38,39] has also been extensively studied. For example, coarse-grained simulations and quantitative experiments have revealed that charged nanoparticles become immobilized in a polymer network with small clusters of oppositely charged nodes, whereas neutral particles were able to freely diffuse.[38] While this study focused on charge–charge interactions, it raises interesting implications for both the utilization of attractive nodes randomly dispersed in a hydrogel and the role of probe interactions with components of the network on probe dynamics. From these studies and others, it is clear that both local polymer density and network heterogeneity as well as interactions between the diffusing species and the network play an important role in nanoparticle dynamics in a hydrogel.

Few studies have focused on the effect of immobile fillers on the dynamics of nanoparticle probes. The filler particles could significantly affect nanoparticle mobility by changing the structure of the hydrogel or by introducing interactions between the filler particle and the nanoparticle probe. While there is previous work studying probe dynamics in polyacrylamide gels, the incorporation of static particles into the hydrogel allows for additional tunability *via* attraction of a nanoprobe to the static particles. Furthermore, while others have detailed the release profile of components such as drugs into or out of nanocomposite hydrogels,[25,26,40] there lacks a fundamental study that examines how the change in structure and interactions influences dynamics of mobile nanoparticle probes at the nanoscale. In particular, these complex systems, both synthetic and biological, are often heterogeneous in nature and creating a model in which both heterogeneity and probe–nanocomposite hydrogel interactions exist concurrently is key to understanding these complex soft matter systems.

This report seeks to understand the influence of immobilized particles on dynamics of a nanoparticle probe in hydrogel nanocomposites. We have chosen to use a single particle tracking (SPT) method to retain the spatial-temporal information of individual probes, necessary for characterizing heterogeneous systems, that would be lost when using a technique that only captures the ensemble average of probe dynamics.[41] Our system consists of static 66 nm silica particles dispersed in polyacrylamide hydrogel with 8 nm poly(ethylene glycol)-grafted quantum dots (PEG-QD) as probe nanoparticles. To produce polyacrylamide

hydrogels with well-dispersed static silica particles, a rapid photopolymerization method is employed. We find that at low concentrations ($\Phi < 0.005$) of silica particles are well dispersed and have minimal effect on the modulus of the gel, indicating that their macroscopic network is not substantially different from that of the neat hydrogel. However, we find that the probes experience different local environments in the hydrogel nanocomposite indicated by that two populations of PEG-QD probes, mobile and localized, compared to the neat hydrogel where the majority of the PEG-QDs are mobile. Using quartz crystal microbalance with dissipation (QCM-D), the localization of the probes is attributed to attraction between the PEG brush on the nanoparticle probe and the silanol group on the silica surface. At high pH, this attraction is turned off and PEG-QDs become predominately mobile in the hydrogel nanocomposite. At higher loadings of static silica particles ($\Phi > 0.01$), the storage modulus decreases consistent with disruption of the hydrogel network. Thus, the increased tortuosity and attractive surfaces which slow dynamics are confounded by the increase in mesh size. Overall, our work demonstrates how probe–particle interactions play an important role in influencing nanoparticle dynamics in a hydrogel nanocomposite.

2 Materials and methods

2.1 Materials

Acrylamide and bisacrylamide are purchased in aqueous solutions from Sigma Aldrich. Lithium phenyl-2,4,6-trimethylbenzoyl-phosphinate (LAP) is purchased from Colorado Photopolymer Solutions. 5 kg mol^{-1} thiol–polyethylene glycol (PEG) is purchased from Creative PEGWorks. Silica particles, Nissan ZL, are generously provided by Nissan (66 nm diameter). Sodium phosphate dibasic dihydrate, sodium dihydrogen phosphate monohydrate, sodium bicarbonate and sodium carbonate are purchased from Sigma Aldrich.

2.2 CdSe/ZnS quantum dots

Oleic acid capped CdSe/ZnS quantum dots (QDs) in toluene are synthesized as described previously[42] and determined to have a core diameter of 3 nm based on transmission electron microscopy (TEM) (see ESI†). To disperse the QDs in water, a ligand exchange using a 5 kg mol^{-1} thiol–PEG is completed as follows.[43] Oleic acid capped QDs are added to a heated (40 °C) thiol–PEG toluene solution, with thiol–PEG in excess and vigorously stirred overnight. PEG-functionalized QDs are precipitated out of solution with the use of a poor solvent (hexane) and centrifuged for 10 minutes at 8500 rpm. The supernatant is discarded and the QD pellet dried before dispersing in either deionized water or buffer solution (10 mL). To remove excess thiol–PEG, the solution is run through a 30 kDa centrifugal filter for 20 minutes at 6200 rpm. The PEG-functionalized QD hydrodynamic diameter is determined to be 8 nm by measuring the diffusion coefficient in solutions of glycerol/water (80, 85, 90 and 95 wt%) at 30 °C and fitting the data to the Stokes–Einstein relationship (see ESI†).

2.3 Silica–polyacrylamide gel synthesis

Solutions of acrylamide (71 g mol^{-1}) and bisacrylamide (154 g mol^{-1}) are prepared in deionized water at 10/0.06% w/v acrylamide/bisacrylamide with increasing concentration of silica particles at a volume fraction, Φ, of 0, 0.005, 0.01 and 0.1. A stock solution of LAP is prepared at a 0.74 wt% and kept away from ambient light. LAP is then added to the pregel acrylamide/bisacrylamide/silica particle solution to achieve a final LAP concentration of 0.067 wt%.[44] The solution is immediately transferred to a 1 mm gap between hydrophobically treated glass slides and irradiated with 10 mW cm^{-2} of UV (Omnicure S1500, 320–390 nm) for three minutes. Following gelation, hydrogels are removed from the glass slides and swollen in either deionized water, sodium phosphate buffer (0.01 M, pH 5.8), or sodium–bicarbonate buffer (0.01 M, pH 9.2) for 48 hours to remove unreacted monomer, crosslinker and initiator. The pH of the buffer solutions are measured using a pH meter prior to use.

PEG-QDs are loaded into the hydrogels following established procedures. Briefly, gels are placed in a 4.4 µg mL^{-1} QD solution, such that the top half of the gel is exposed to air to promote QD infiltration *via* evaporation.[27] After infiltration, gels are fully immersed in the QD rich solution. Experiments are performed 24 h after the full immersion to ensure that the hydrogels have fully equilibrated.

2.4 Silica–polyacrylamide gel characterization

Oscillatory *in situ* rheometry is performed on an AR2000ex (TA Instruments) fitted with an aluminium cone (0° 59′ 42″ angle, 22 mm diameter) and plate geometry with a light guide connected to a UV lamp (Omnicure S1500, 320–390 nm) that irradiated the sample through a quartz plate. After the solution is equilibrated for 30 seconds (1% strain, 10 rad s^{-1}), a time sweep during and after polymerization is conducted, with the gel irradiated with 10 mW cm^{-2} of UV for three minutes. The gels are maintained within the linear regime as determined prior to the measurements using a strain sweep from 0.5 to 5% at 10 rad s^{-1}. A frequency sweep from 1 to 20 rad s^{-1} at a strain of 1% is used to determine the zero shear storage modulus, $G'_{(0)}$, for mesh size characterization (see ESI†). All gels are polymerized in a solvent trap to ensure there is no change in the network due to evaporation.

For scanning electron microscopy (SEM) (Quanta 600 FEG ESEM), hydrogels are swollen in deionized water to equilibrate before lyophilizing overnight and subsequently fracturing the gel to expose a cross section of the gel. The exposed cross-sections are then imaged under low-vacuum (0.53 torr, 5 kV). Additionally, lyophilization of swollen gels is also used to determine the polymer volume fraction, used in mesh size calculations.

2.5 Single particle tracking (SPT) and analysis

Quantum dot (QD) dynamics within the silica–polyacrylamide hydrogels is imaged using an inverted Nikon Eclipse Ti optical microscope equipped with a 100×, 1.49 NA oil immersion objective (Nikon). Videos of a 512 × 512 pixel region of interest are collected for 40 seconds, at 25 frames per second, using a cooled EMCCD camera (Evolve-512, Photometrics). Particle trajectories are determined using Fluorescence Image Evaluation Software for Tracking and Analysis (FIESTA), which utilizes a 2-D Gaussian fit for particle localization.[45] Blinking of QDs indicates that the QDs are single particles rather than aggregates, and a maximum break of 4 frames is allowed in the tracking analysis to accommodate blinking and samples are kept solvated to ensure there are no changes in the network due to evaporation. Mean squared displacements (MSD) are calculated using msdanalyzer in MATLAB.[46]

The mean squared displacement (MSD) of a particle, or the square of the net distance a particle travels, is described by

$$\text{MSD}(\tau) = \langle \Delta r(\tau)^2 \rangle_t = \langle [r(t + \tau) - r(t)]^2 \rangle_t \tag{1}$$

where τ is the lag time, $r(t)$ is the position of the particle at absolute time t, and $\langle \rangle_t$ denotes the averaging over time. The displacements of each particle motion is determined by

$$\Delta x = x(\tau + \tau_i) - x(\tau) \tag{2}$$

where τ_i is the time interval between positions and Δx represents the displacements in both x and y.

2.6 Quartz crystal microbalance with dissipation (QCM-D)

The adsorption of the PEG-QDs onto a silica coated crystal is determined using QCM-D, performed on a QSense analyzer (QSense, Gothenburg, Sweden). Prior to use, crystals are cleaned with a 2% w/v sodium dodecyl sulfate solution, rinsed with deionized water, and placed under UV-Ozone for ten minutes to remove any impurities. Cleaned crystals are then immediately equilibrated overnight in either sodium phosphate or sodium carbonate–bicarbonate buffer to achieve a stable baseline. PEG-QDs are introduced into the flow cell at a flow rate of 50 µL min^{-1} at 22 °C in a PEG-QD rich buffer solution (0.055 mg mL^{-1}). This concentration is chosen by measuring the change in resonance frequency for multiple solution concentrations and determining for what concentration there was no further change in the resonance frequency, corresponding to full surface coverage of the crystal.

3 Results and discussion

This study analyzes the effect of probe–particle interactions on the dynamics of 8 nm PEG brush functionalized quantum dot (QD) nanoparticles (8 nm hydrodynamic diameter: 3 nm CdSe/ZnS core) in silica–polyacrylamide gels as a function of silica (66 nm diameter) particle loading and pH using single particle tracking (SPT) methods. Silica–polyacrylamide hydrogel nanocomposites are synthesized using a photoinitiator at four different silica particle concentrations, Φ = 0, 0.005, 0.01 and 0.1. The use of LAP as a photoinitiator, rather than the commonly used ammonium persulfate (APS) and N,N,N',N'-tetramethylethylenediamine (TEMED) initiator and accelerator combination, facilitates homogeneous dispersion of silica particles. Scanning electron microscopy (SEM) and rheology are used to

characterize particle dispersion within the network and the macroscopic changes to the network reflected by changes in the storage modulus (G'). The extent of PEG-QD probe and static silica particle interactions at different pHs is measured using quartz crystal microbalance with dissipation (QCM-D).

3.1 Characterization of silica–polyacrylamide hydrogel

To characterize the nanoscale environment of the probe, the hydrogel mesh size in the neat system and the dispersion of the silica particles is characterized. First, the average mesh size, $\langle\zeta\rangle$, is determined as a function of acrylamide concentrations by measuring the zero-shear storage modulus, ($G'_{(0)}$), and dried polymer volume fraction, v_p. To study probe dynamics in gels, $\langle\zeta\rangle$ should ideally be larger than the diameter of the PEG-QD (8 nm) so that the probe nanoparticles are not trapped in the hydrogel mesh. Additionally, the $\langle\zeta\rangle$ should be smaller than that of the static silica particles (66 nm), to ensure that the silica particles are immobilized after gelation. For the synthesized hydrogels, a starting composition of 10/0.06% w/v best meets these criteria with an average mesh size of 25 nm (see ESI†). Relative sizes of the network, silica particles, and probe nanoparticles are illustrated in a schematic in Fig. 1.

To determine the extent of silica particle dispersion, the cross section of bulk samples, created by fracturing lyophilized hydrogels, are imaged using scanning electron microscopy (SEM) (Fig. 2). For low to moderate loadings (Φ = 0.005, 0.01) the silica particles are well dispersed in the lyophilized gels. For higher loading (Φ = 0.1), the particles are closely spaced in the lyophilized gel which makes it difficult to determine if particles are well dispersed in the hydrated state. The excellent dispersion of silica particles at low and moderate loadings can be partly attributed to the rapid gelling of the polyacrylamide network. Conventionally, polyacrylamide gels are chemically polymerized using APS and TEMED.[3] To achieve the desired mesh size for this system, the corresponding acrylamide monomer concentration would require gelation on the time scale of tens of minutes. In this study, we use the fast gelation kinetics of photopolymerization, in which the onset of network formation
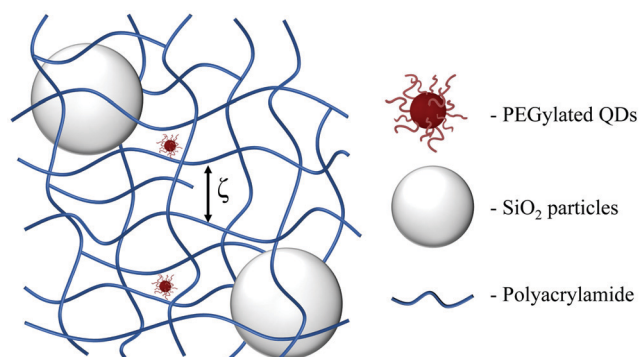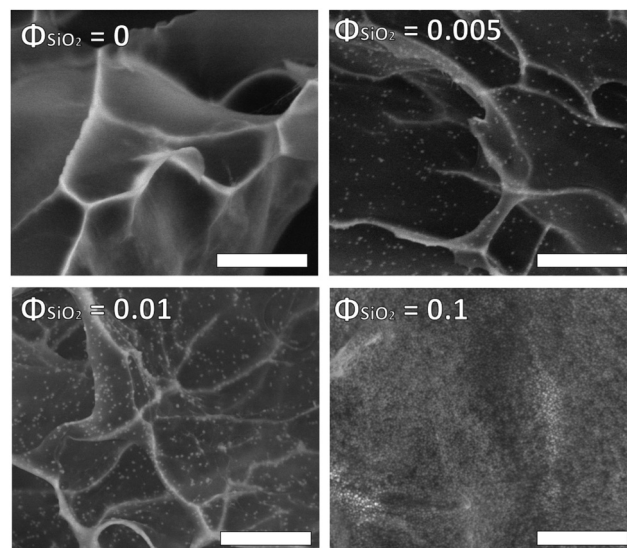

Fig. 2 SEM images of lyophilized cross-sections of silica–polyacrylamide hydrogels showing silica particle dispersion. The white lines are fracture surfaces. Scale bars are 3 μm.

occurs rapidly (<1 minute) as characterized by the crossover point of storage (G') and loss (G'') shear modulus. In this case, the network is formed within tens of seconds which corresponds to the emergence of a plateau of the storage modulus, G'_p (Fig. 3). The rapid gelation kinetics limits the movement of silica particles during polymerization and traps them in a desired dispersed state. As shown in ESI,† the slow kinetics in the chemical cross-linking method induces aggregation of silica particles even at moderate concentrations.

In this study, rheology is conducted with two aims: (1) to measure an average mesh size of the neat hydrogel and (2) to
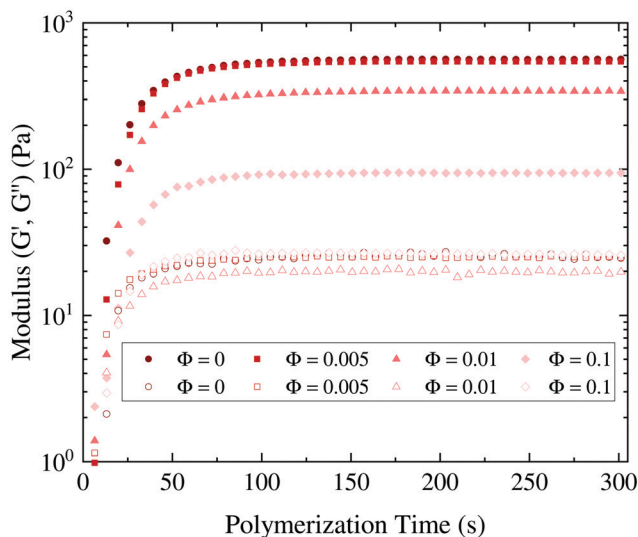

Fig. 1 Schematic showing the key length scales of the system. The hydrogel nanocomposite consists of static silica particles, 66 nm diameter, in a polyacrylamide network with average mesh size $\langle\zeta\rangle$ = 25 nm. Hydrodynamic diameter of PEG-QDs is 8 nm.

Fig. 3 Storage modulus (G'), closed symbols, and loss modulus (G''), open symbols, of polyacrylamide gels with silica particle loadings from Φ = 0 to 0.1 as a function of time after exposure to UV light at time 0 (320–390 nm, 10 mW cm^{-2}). Samples are irradiated from time = 0 to time = 180 seconds.

determine if the introduction and dispersion of silica at different loading concentrations impacts the network properties at a macroscopic level. For all cases, the loss modulus, G'', is below the storage modulus, G', prior to initiation, shown as time 0 in (Fig. 3). Almost immediately the loss modulus is overtaken by the storage modulus ($G' > G''$) upon UV exposure, indicating the rapid onset of network formation. The storage modulus in all cases begins to plateau after one minute indicating that network formation is complete within the three minute irradiation period. Additionally, there is no appreciable change in the gelation time, quantified by both the crossover of G' and G'' and the time for G' to plateau, approximately 15 seconds and 90 seconds, respectively, with increasing silica volume fraction. This indicates that the presence of silica particles does not dramatically affect reaction kinetics.

While there is not a drastic change in the plateau storage modulus, G'_p, for low loadings of silica particles ($\Phi = 0.005$) compared to the neat hydrogel (544 and 562 Pa, respectively), there is a pronounced decrease in G'_p for higher loadings of silica ($\Phi = 0.05, 0.1$) to 340 and 94 Pa, respectively, though there is no appreciable change in the macroscopic swelling of the network. As the storage modulus is a measure of the number of elastically deformable chains in a network, a decrease in G'_p at higher particle loadings indicates a disruption of the polymeric mesh. In this system, a plausible explanation for the decrease in G'_p is that the disruption of the polymeric mesh, caused by the silica particles inhibiting the gelation process, outweighs any potential reinforcement effects.[47] A previous study has found that incorporating silica and polystyrene nanoparticles into poly(N-isopropylacrylamide) (pNIPAAm) hydrogels using photopolymerization caused defects around the nanoparticles (i.e. dangling chains) above $\Phi = 0.015$, similar to the defects we anticipate in our polyacrylamide hydrogels with moderate to high silica loadings.[48] This change must be considered when evaluating the effect of silica loading on probe dynamics.

3.2 Single particle tracking (SPT) in hydrogel nanocomposites

Single particle tracking (SPT) is used to determine the displacement and MSDs of PEG-QD probes as a function of silica particle loading. Fig. 5 (top) shows the MSD of individual PEG-QD tracks as well as the ensemble averaged MSD given by the solid black line for gels with $\Phi = 0$, 0.005, 0.01 and 0.1 of silica particles. To better visualize the distribution of MSDs, as well as quantify the mobile *versus* localized PEG-QD populations, Fig. 4 (bottom row) shows the normalized distribution of MSDs at a lag time of $\tau = 0.2$ s, indicated by the dashed black line in Fig. 4 (top row). This time scale is large enough to visualize extended tracks, observe the spread of MSDs due to mobile and localized populations, and provide good statistics. Using the lower boundary of the neat gel as a guide, we define mobile particles as those having displacements greater than 200 nm after 0.2 s. In Fig. 4 (bottom) this boundary separates the orange (localized) and blue (mobile) regimes. In the neat polyacrylamide gel, the majority of the PEG-QDs are mobile (92%) which is expected given the size of the PEG-QD compared to the average mesh size.[28,43] While there is variability in the value of individual MSDs, this is expected given the underlying nanoscale heterogeneity of the polyacrylamide hydrogel that has been extensively studied by others.[27,28,49]

As small loadings of static silica particles are added, $\Phi = 0.005$, there is an emergence of a second, localized population at low values of MSD. While this can be seen in the individual PEG-QD tracks (Fig. 4, top), the large number of overlapping particle tracks make it more distinctive in the distribution of MSDs (Fig. 4, bottom). Correspondingly, there is a drop in the percentage of mobile PEG-QD probes, from 92 to 63%. As more silica is added, $\Phi = 0.01$ and 0.1, there are still two distinct populations of PEG-QD probes. However, the percentage of mobile PEG-QDs remains relatively constant, 60% and 63%, respectively.

While the MSDs detail the dynamics of probe motion, the distribution of displacements gives more information about
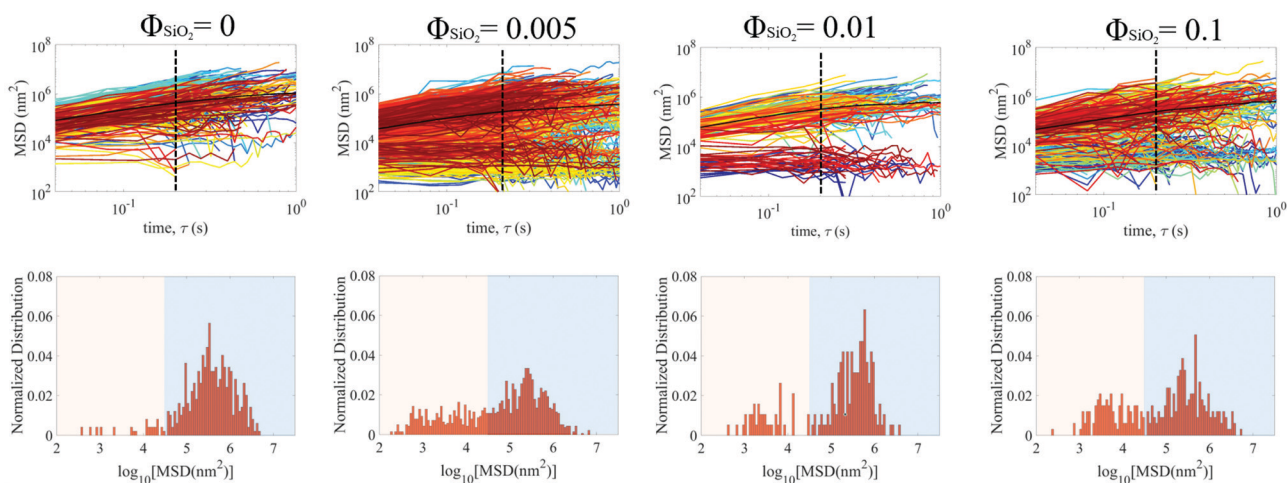

Fig. 4 Mean-squared displacements (MSD) (top row) and normalized distribution of MSD (bottom row) of individual particle trajectories for increasing silica concentrations. Dashed line is a guide to the eye for $\tau = 0.2$ seconds and solid black line indicates the ensemble-averaged MSD (top row). Shading (bottom row) delineates mobile and localized particle populations.

the structural heterogeneity of the system. To examine this, the van Hove correlation function $p(\Delta x, \tau)$ can be used, which details the probability of finding a probe at a certain displacement for a given lag time, τ, allowing for the separation of slow and fast dynamics. For monodisperse probes diffusing through a homogeneous matrix, the van Hove distribution takes the form of a Gaussian. However, for probes moving through heterogeneous matrices resulting in different local dynamics, the van Hove is expected to deviate from the Gaussian functional form with the emergence of long exponential tails. These exponential tails have been observed both computationally and experimentally in a variety of systems including glassy materials, entangled polymer solutions, and hydrogels.[27,50–53] These tails, corresponding to large displacements, are quantified by the decay length, $\lambda(\tau)$, of the probe for that particular τ when fitted with an exponential function:

$$p(\Delta x, \tau) \sim \exp(-|\Delta x|/\lambda(\tau)) \qquad (3)$$

Fig. 5 (top) shows the van Hove correlation function $p(\Delta x, \tau)$ for $\Phi = 0.005$ for increasing τ. The van Hove distributions exhibit two distinct populations, consistent with the MSD distributions in Fig. 4. For small displacements, the distribution is well described by a Gaussian, representing the localized population of PEG-QDs below the tracking localization resolution.
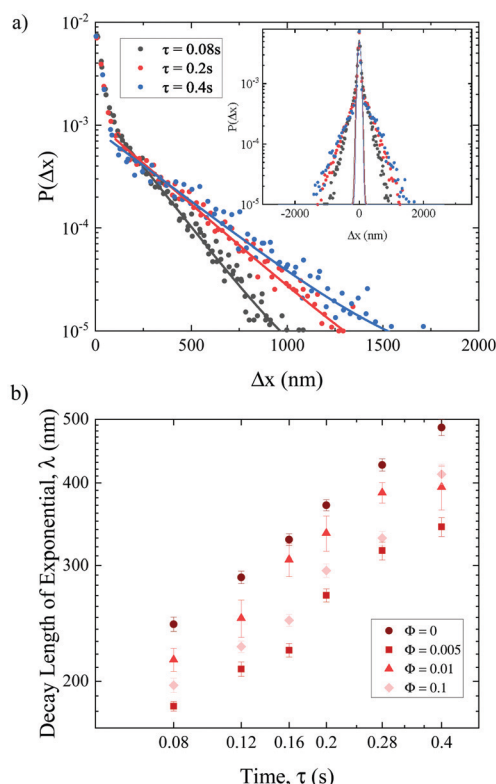
In contrast, the large, relatively rare, displacements cannot be described by a Gaussian but are better described by an exponential, eqn (3). In other hydrogels, these large displacements are attributed to a probe escaping from local cages and freely diffusing before becoming trapped in another cage formed by either the hydrogel mesh or larger scale structural features.[27,54] Fig. 5(b) shows that $\lambda(\tau)$ increases as τ increases for all loadings. For example, in the neat polyacrylamide ($\Phi = 0$), $\lambda(\tau)$ increases from 250 to 450 nm as τ increases from 0.08 to 0.4 s, respectively. Additionally, for all τ, $\lambda(\tau)$ is the largest in the neat polyacrylamide indicating that static particles slow probe mobility. Furthermore, a power-law dependence describes $\lambda(\tau)$ *versus* τ, with a power-law exponent of 0.38, in agreement with the previously reported value of 0.33 for a variety of polyacrylamide gels.[27]

Interestingly, at a fixed τ, the change in decay length with silica loading is non-monotonic. Specifically, upon initial addition of silica, $\Phi = 0.005$, there is a marked decrease in the $\lambda(\tau)$ at each τ. For example, at $\tau = 0.2$ s, the decay length decreases from 370 nm for $\Phi = 0$ to 270 nm for $\Phi = 0.005$. However, as silica loading increases further, the $\lambda(\tau)$ increases ($\Phi = 0.01$) and then again decreases ($\Phi = 0.1$). This is unexpected, as increasing concentration of silica would lead to a decrease in particle mobility if the mesh size is unperturbed because the silica particles take up space in the hydrogel acting as obstructions. A similar decrease of $\lambda(\tau)$ is observed in polyacrylamide gels when the polymer or crosslinker concentration is increased, which is attributed to an increased number or more restrictive probe traps.[27] This non-monotonic trend in the $\lambda(\tau)$ may be explained by the change in the network structure for the moderate and high loadings. For these loadings, a decrease in G'_p correlates with fewer elastically deformable chains contributing to the network. This decrease suggests a larger mesh size (faster probe mobility), but interestingly, the log-normal mean is not substantially changed for all silica particle loadings when comparing the mobile populations (see ESI†). This observation may indicate that a more open network, as suggested by the decrease in G', may not measurably change the MSD due to relative sizes between the QD-PEG (8 nm) and the hydrogel mesh (25 nm). Another explanation could be that the addition of silica only disrupts the network region localized around the particles, similar to the defects observed in other UV polymerized hydrogel nanocomposites.[48]

We attribute the trend in $\lambda(\tau)$ to the confounding influence of tortuosity, probe–immobile particle interactions and network defects on probe dynamics. Namely, $\lambda(\tau)$ at $\Phi = 0.01$ is larger than that at 0.005 likely because network defects dominate (*i.e.*, relative increase in silica loading is 2×). For $\Phi = 0.1$, $\lambda(\tau)$ is reduced because we believe tortuosity and attraction dominates the probe dynamics (*i.e.* relative increase in silica loading is 10×). Further studies are needed to identify the location of network defects upon addition of silica particles, which is beyond the scope of the present study. We therefore propose that at loadings of $\Phi = 0.01$ and 0.1, the addition of silica particles changes the network structure as illustrated in the schematic shown in Fig. 6. At the lowest loading of static

Fig. 5 (a) Van Hove correlation functions for $\Phi = 0.005$ silica for various lag times, τ. Curves are exponential fits. Inset shows Gaussian fit of small displacements. (b) Characteristic decay length of the exponential tail λ for increasing τ at various silica loadings. Error bars associated with error of fitting the exponential decay to the van Hove distribution.
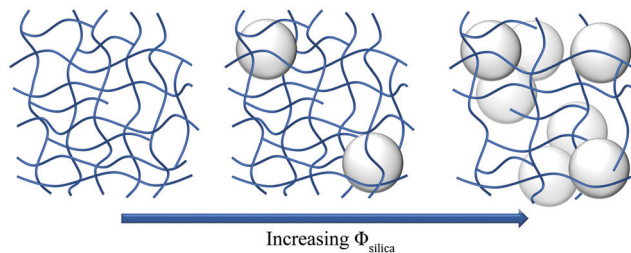
Fig. 6 Schematic detailing the microscopic changes to the hydrogel mesh with the incorporation of silica particles. Neat hydrogel (left). As small loadings of silica are added, Φ = 0.005, the mesh structure is not appreciably changed and silica particles are dispersed (middle). As higher loadings of silica are added, Φ = 0.01 and 0.1, the mesh structure is disrupted and silica particles may aggregate (right).

silica, Φ = 0.005, the silica particles are dispersed throughout the hydrogel with no appreciable changes in the mesh structure as indicated by rheology but as additional silica is added the network is disrupted. The low loading case is particularly interesting, as there are no appreciable macroscopic rheological changes in structure, but a clear emergence of two distinct PEG-QD populations as seen in particle tracking. Thus, the low loading hydrogel provides a well-defined system to explore the role of PEG-QD interactions with the immobile silica particles on the dynamics of the probe particles in this system, mediated by pH. We focus on understanding the Φ = 0.005 case to investigate how static silica particles in an unperturbed network impacts PEG-QD dynamics.

3.3 Effect of attractive interactions between PEG-QD and silica particles on probe mobility

The localized PEG-QD population can arise from attractive interactions between the PEG-QDs and the silica particles. Interactions between PEG and silica have been well established in the literature.[55–62] Specifically, an attractive interaction between PEG and silica can arise from hydrogen bonding between the oxygen in the PEG backbone and the hydrogen of the silanol on the silica surface at neutral to slightly acidic pH. At high pH, the silanol deprotonates and as a result the adsorption of the PEG brush to the silica surface is not expected. To confirm and quantify the extent of PEG–silica interactions, the adsorption of PEG-QD to silica surfaces are investigated using QCM-D at pH 5.8 and pH 9.2 to probe both of the above mentioned regimes.

At low pH, Fig. 7 shows that the resonance frequency decreases to $\sim$40 Hz and plateaus after 20 minutes. Correspondingly, the dissipation increases to a value of 3×10^{-6}. Conversely, at high pH for the same exposure time, there is a negligible change in the resonance frequency compared to the low pH. The large decrease in F for the 3rd overtone ($\sim$40 Hz) indicates that there is adsorption of the PEG-QDs on the surface in the low pH case, with little to no adsorption ($\sim$0.5 Hz) of the PEG-QDs onto the surface for the high pH. A slight increase in D at high pH ($\sim 0.1 \times 10^{-6}$), can be attributed to the change in viscosity upon changing the medium from pure buffer to the PEG-QD solution. We therefore conclude that at pH 5.8, there is
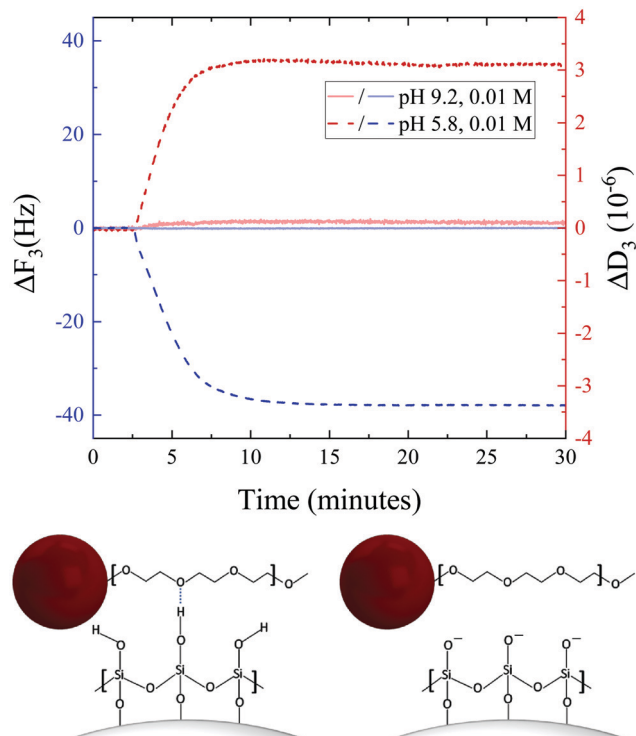

Fig. 7 Change in frequency (ΔF, blue) and dissipation (ΔD, red) as a silica coated QCM-D crystal is exposed to a PEG-QD solution (top). Experiments are conducted in solutions with pH 9.2 (solid lines) and pH 5.8 (dashed lines). 3rd overtone is shown, but other overtones (5–13) follow the same trend (see ESI†). Schematic illustrating hydrogen bonding interaction between PEG-QD and silica surface at low (left) and high (right) pH (bottom).

an attractive interaction between the PEG-QD and the silica surface and a negligible interaction at pH 9.2, due to hydrogen bonding interactions between the PEG backbone of the PEG-QD and the silanol on the surface of the silica crystal. We now explore how this attractive interaction modifies PEG-QD dynamics within the hydrogel composite.

To determine the effect of pH-mediated interactions on the dynamics of a probe, SPT is used to study PEG-QD dynamics in gels loaded with Φ = 0.005 of silica particles, which have uniform distribution of static silica particles and similar storage modulus as the neat gel. Polyacrylamide networks themselves are not expected to be pH sensitive because they are made solely of acrylamide. At pH 5.8, where hydrogen bonding between the PEG-QD and silica are present, all probes are localized on experimental time scales (Fig. 8(a)). This restriction on probe displacement is consistent with the QCM-D results, where PEG-QDs adsorbed onto the surface of the silica crystal at pH 5.8. Conversely, when there is limited interaction between the particle surface and probe, in this case at pH 9.2, a large fraction of PEG-QDs are mobile, 91% (Fig. 8(b)). As in our prior studies (Fig. 4), a displacement of larger than 200 nm is used as the cut-off for determining mobile and localized probe mobility. This behavior is further quantified by examining the distributions of MSDs of individual probes trajectories in each of these cases at τ = 0.2 s (Fig. 8(c)), which clearly showcases a drastic reduction in the range
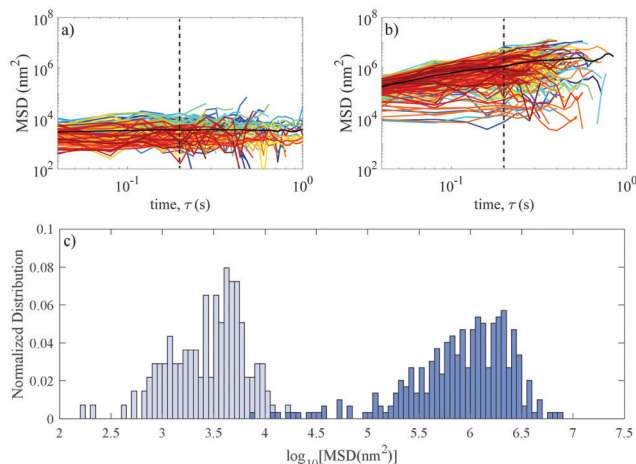
Fig. 8 MSDs for individual PEG-QDs in a Φ = 0.005 silica-acrylamide hydrogel for pH 5.8 (a) and pH 9.2 (b). Dashed line is a guide to the eye for τ = 0.2 seconds. (c) Normalized distribution of MSDs for both pH 5.8 (light blue) and pH 9.2 (dark blue) at τ = 0.2 seconds.
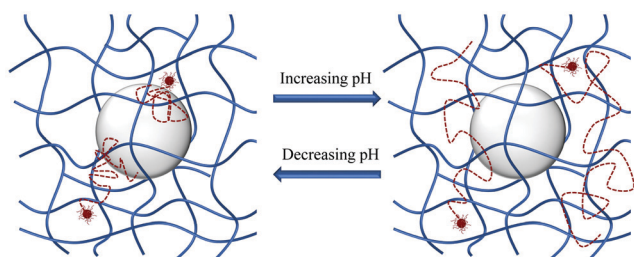

Fig. 9 Schematic detailing the effect of pH on the mobility of PEG-QD probes within a polyacrylamide−silica hydrogel (Φ = 0.005) at acidic (left) and basic (right) pHs.

of MSDs for the pH 5.8 (light blue) *versus* the pH 9.2 (dark blue) case. We illustrate the change in probe mobility with varying pH in Fig. 9, where PEG-QD motion is localized to the surface of the silica particle (left, top QD), or adjacent to the silica particle (left, lower QD). Conversely, at high pH when there is no attraction between the silica and PEG-QDs, the PEG-QD only weakly interacts with the static silica particles. In this case, the PEG-QD explores the surrounding mesh of the polyacrylamide gel. Thus, increasing pH can lead to increased probe mobility whereas decreasing pH induces localized and trapped motion. This ability to tune the dynamics at the nanoscale by introducing static silica particles and by controlling the surface area of the attractive nodes can be utilized in separation technologies or to modulate drug release from hydrogel nanocomposite involving pH sensitive systems. For example, the release of active agents from a hydrogel can be modulated without changing the overall mechanical properties of the hydrogel, which may find important applications in tissue engineering.

4 Conclusions

In this study, static silica particles are incorporated into poly-acrylamide hydrogels to determine their effect on PEG-QD probe dynamics. Photopolymerization is used to trap the silica particles homogeneously throughout the hydrogel. At low loadings, Φ = 0.005, the addition of silica particles results in the emergence of mobile and localized populations of PEG-QDs dynamics in the hydrogel nanocomposite compared to the neat hydrogel in which the PEG-QDs are primarily mobile. At higher loadings, this effect is confounded by the change in macroscopic properties, namely a reduction in the storage modulus. Because it exhibits nearly the same storage modulus as the near gels, the Φ = 0.005 hydrogel serves as a model system to investigate the effect of probe–particle interactions on PEG-QD dynamics. To quantify probe–particle interactions, QCM-D shows that at pH 5.8 there is an attractive interaction between the PEG brush of the QD and the silica surface, with negligible interactions at pH 9.2. This in turn impacts particle dynamics in the gels in each of these regimes, as particles are mobile at pH 9.2 but localized at pH 5.8. The findings of this study highlight the importance of accounting for the interactions between a probe and the all components of the matrix, and shows that in these complex systems where both interactions and heterogeneity impact particle dynamics, interactions between the probe and matrix components can dominate over net-work heterogeneity. Our study adds to the previous work in understanding nanoparticle dynamics in hydrogels, including polymer concentration, mesh size and probe-polymer interactions, which allows for a more complete understanding of probe dynamics in hydrogel nanocomposites. Ultimately, this study can serve as a springboard to investigate more complex systems in which probe–particle and heterogeneity exist, such as biofilms, and can inform how to design hydrogel nanocomposites for applications including drug delivery and nanoscale filtration, as well as motivation to examine the effect of probe concentration in similar systems.

Conflicts of interest

There are no conflicts to declare.

Acknowledgements

Notes and references

1 S. K. Seidlits, Z. Z. Khaing, R. R. Petersen, J. D. Nickels, J. E. Vanscoy, J. B. Shear and C. E. Schmidt, *Biomaterials*, 2010, **31**, 3930–3940.

2 J. R. McKee, S. Hietala, J. Seitsonen, J. Laine, E. Kontturi and O. Ikkala, *ACS Macro Lett.*, 2014, **3**, 266–270.

3 J. R. Tse and A. J. Engler, *Curr. Protoc. Cell Biol.*, 2010, **47**, 10.16.1–10.16.16.

4 K. Haraguchi and T. Takehisa, *Adv. Mater.*, 2002, **14**, 1120–1124.

5 E. Karadağ, D. Saraydin, S. Çetinkaya and O. Güven, *Biomaterials*, 1996, **17**, 67–70.

6 P. Calvert, *Adv. Mater.*, 2009, **21**, 743–756.

7 S. Khetan, J. S. Katz and J. A. Burdick, *Soft Matter*, 2009, **5**, 1601–1606.

8 P. Matricardi, C. Di Meo, T. Coviello, W. E. Hennink and F. Alhaique, *Adv. Drug Delivery Rev.*, 2013, **65**, 1172–1187.

9 C. H. Park and I. Orozco-Avila, *Biotechnol. Prog.*, 1992, **8**, 6.

10 Y. Wang, J. Wang, Z. Yuan, H. Han, T. Li, L. Li and X. Guo, *Colloids Surf., B*, 2017, **152**, 252–259.

11 O. Ozay, S. Ekici, Y. Baran, S. Kubilay, N. Aktas and N. Sahiner, *Desalination*, 2010, **260**, 57–64.

12 B. A. Getachew, S.-R. Kim and J.-H. Kim, *Environ. Sci. Technol.*, 2017, **51**, 905–913.

13 B. Kar-On Leung and G. Robinson, *J. Membr. Sci.*, 1990, **52**, 1–18.

14 E. L. Cussler, M. R. Stokar and J. E. Varberg, *AIChE J.*, 1984, **30**, 578–582.

15 E. Parrish, S. C. Seeger and R. J. Composto, *Macromolecules*, 2018, **51**, 3597–3607.

16 F.-J. Xu, E.-T. Kang and K.-G. Neoh, *Biomaterials*, 2006, **27**, 2787–2797.

17 M. Cao, Y. Wang, X. Hu, H. Gong, R. Li, H. Cox, J. Zhang, T. A. Waigh, H. Xu and J. R. Lu, *Biomacromolecules*, 2019, **20**, 3601–3610.

18 R. E. Kohman, C. Cha, S. C. Zimmerman and H. Kong, *Soft Matter*, 2010, **6**, 2150–2152.

19 M. Y. Abdelaal, E. A. Abdel-Razik, E. M. Abdel-Bary and I. M. El-Sherbiny, *J. Appl. Polym. Sci.*, 2007, **103**, 2864–2874.

20 M. Krogsgaard, M. A. Behrens, J. S. Pedersen and H. Birkedal, *Biomacromolecules*, 2013, **14**, 297–301.

21 D. Costa, A. J. M. Valente, M. G. Miguel and J. Queiroz, *Langmuir*, 2011, **27**, 13780–13789.

22 Z. Zheng, J. Hu, H. Wang, J. Huang, Y. Yu, Q. Zhang and Y. Cheng, *ACS Appl. Mater. Interfaces*, 2017, **9**, 24511–24517.

23 S.-H. Hu, T.-Y. Liu, D.-M. Liu and S.-Y. Chen, *Macromolecules*, 2007, **40**, 6786–6788.

24 N. S. Satarkar and J. Z. Hilt, *J. Controlled Release*, 2008, **130**, 246–251.

25 Y. Wang, B. Li, F. Xu, Z. Han, D. Wei, D. Jia and Y. Zhou, *Biomacromolecules*, 2018, **19**, 3351–3360.

26 H. J. Jung, M. Abou-Jaoude, B. E. Carbia, C. Plummer and A. Chauhan, *J. Controlled Release*, 2013, **165**, 82–89.

27 C. H. Lee, A. J. Crosby, T. Emrick and R. C. Hayward, *Macromolecules*, 2014, **47**, 741–749.

28 E. Parrish, M. A. Caporizzo and R. J. Composto, *J. Chem. Phys.*, 2017, **146**, 203318.

29 K. Forier, A.-S. Messiaen, K. Raemdonck, H. Deschout, J. Rejman, F. De Baets, H. Nelis, S. C. De Smedt, J. Demeester, T. Coenye and K. Braeckmans, *Nanomedicine*, 2012, **8**, 935–949.

30 S. Fulaz, H. Devlin, S. Vitale, L. Quinn, J. P. O'Gara and E. Casey, *Int. J. Nanomed.*, 2020, **15**, 4779–4791.

31 B. A. Nevius, Y. P. Chen, J. L. Ferry and A. W. Decho, *Ecotoxicology*, 2012, **21**, 2205–2213.

32 K. Ikuma, A. W. Decho and B. L. T. Lau, *Front. Microbiol.*, 2015, **6**, 1–8.

33 T.-O. Peulen and K. J. Wilkinson, *Environ. Sci. Technol.*, 2011, **45**, 3367–3373.

34 E. Rascol, J.-M. Devoisselle and J. Chopineau, *Nanoscale*, 2016, **8**, 4780–4798.

35 J. K. Vasir and V. Labhasetwar, *Biomaterials*, 2008, **29**, 4244–4252.

36 A. Gesper, P. Hagemann and P. Happel, *Nanoscale*, 2017, **9**, 14172–14183.

37 A. Verma and F. Stellacci, *Small*, 2010, **6**, 12–21.

38 J. Hansing, J. R. Duke, E. B. Fryman, J. E. DeRouchey and R. R. Netz, *Nano Lett.*, 2018, **18**, 5248–5256.

39 V. Adibnia and R. J. Hill, *Polymer*, 2017, **112**, 457–465.

40 N. N. Reddy, K. Varaprasad, S. Ravindra, G. V. S. Reddy, K. M. S. Reddy, K. M. Mohan Reddy and K. M. Raju, *Colloids Surf., A*, 2011, **385**, 20–27.

41 K. A. Rose, M. Molaei, M. J. Boyle, D. Lee, J. C. Crocker and R. J. Composto, *J. Appl. Phys.*, 2020, **127**, 191101.

42 M. Cargnello, B. T. Diroll, E. A. Gaulding and C. B. Murray, *Adv. Mater.*, 2014, **26**, 2419–2423.

43 E. Parrish, K. A. Rose, M. Cargnello, C. B. Murray, D. Lee and R. J. Composto, *Soft Matter*, 2020, **16**, 2256–2265.

44 L. A. Sawicki and A. M. Kloxin, *J. Visualized Exp.*, 2016, 1–10.

45 F. Ruhnow, D. Zwicker and S. Diez, *Biophys. J.*, 2011, **100**, 2820–2828.

46 N. Tarantino, J.-Y. Tinevez, E. F. Crowell, B. Boisson, R. Henriques, M. Mhlanga, F. Agou, A. Israël and E. Laplantine, *J. Cell Biol.*, 2014, **204**, 231–245.

47 L. WuLingzi, L. Zeng, H. Chen and C. Zhang, *Polym. Bull.*, 2011, **68**, 309–316.

48 M. Yanagioka and C. W. Frank, *Langmuir*, 2009, **25**, 5927–5939.

49 N. Orakdogen and O. Okay, *J. Appl. Polym. Sci.*, 2007, **103**, 3228–3237.

50 B. Wang, S. M. Anthony, S. C. Bae and S. Granick, *Proc. Natl. Acad. Sci. U. S. A.*, 2009, **106**, 15160–15164.

51 R. Colin, A. M. Alsayed, J.-C. Castaing, R. Goyal, L. Hough and B. Abou, 2011, arXiv:1010.5087 [cond-mat].

52 P. Chaudhuri, Y. Gao, L. Berthier, M. Kilfoil and W. Kob, *J. Phys.: Condens. Matter*, 2008, **20**, 244126.

53 B. P. Bhowmik, I. Tah and S. Karmakar, *Phys. Rev. E*, 2018, **98**, 022122.

54 M. T. Valentine, P. D. Kaplan, D. Thota, J. C. Crocker, T. Gisler, R. K. Prud'homme, M. Beck and D. A. Weitz, *Phys. Rev. E: Stat., Nonlinear, Soft Matter Phys.*, 2001, **64**, 061506.

55 X. Zeng and K. Osseo-Asare, *Colloids Surf., A*, 2003, **226**, 45–54.

56 W. Walker Jr., J. Reed, S. Verma and W. Zirk, *J. Am. Ceram. Soc.*, 1999, **82**, 585–590.

57 S. Mathur and B. M. Moudgil, *J. Colloid Interface Sci.*, 1997, **196**, 92–98.

58 O. Neel, G. Ducouret and F. Lafuma, *J. Colloid Interface Sci.*, 2000, **230**, 244–253.

59 E. Koksal, R. Ramachandran, P. Somasundaran and C. Maltesh, *Powder Technol.*, 1990, **62**, 253–259.

60 E. Killmann, *Polymer*, 1976, **17**, 864–868.

61 R. L. Derosa and J. A. Trapasso, *J. Mater. Sci.*, 2002, **37**, 1079–1082.

62 S. R. Raghavan, H. J. Walls and S. A. Khan, *Langmuir*, 2000, **16**, 7920–7930.